A divergent CheW confers plasticity to nucleoid-associated chemosensory arrays

Annick Guiseppi[1*], Juan Jesus Vicente[2*], Aurelie Barneoud[1*], Audrey Moine[1], Leon Espinosa[1], Marie-Jeanne Basse[3], Virginie Molle[4], Tâm Mignot[1], Philippe Roche[3] and Emilia M.F. Mauriello[1#]

[1] Aix Marseille Univ, CNRS, LCB, Marseille, France; [2]Physiology & Biophysics, University of Washington, Seattle, WA, USA; [3]CNRS, INSERM, Aix Marseille Univ, Institute Paoli-Calmettes, CRCM, Marseille, France; [4]Montpellier II et I University, CNRS, Laboratoire de Dynamique des Interactions Membranaires Normales et Pathologiques, France.

[*] These authors contributed equally

[#]Correspondence to:
Emilia M.F. Mauriello
Aix Marseille Univ, CNRS, LCB
31 Chemin Joseph Aiguier, Marseille, 13402, France
Tel. +33491164321
Email : emauriello@imm.cnrs.fr

Running Title: The *Myxococcus xanthus* FrzB CheW-like protein acts upstream of the Frz chemotaxis pathway

ABSTRACT

Chemosensory systems are highly organized signaling pathways allowing bacteria to adapt to environmental changes. The Frz chemosensory system from *M. xanthus* possesses, in addition to its core CheW, FrzA, a second CheW homologue, FrzB. We found that this protein does not interact with the cognate CheA, FrzE, as it lacks the amino acid region responsible of this interaction. FrzB, instead, acts upstream of FrzCD in the regulation of *M. xanthus* chemotaxis behaviors and activates the Frz pathway by allowing the formation and distribution of multiple chemosensory clusters on the nucleoid. These results, together, show that the lack of the CheA-interacting region in FrzB confers new functions to this small protein.

INTRODUCTION

Chemosensory systems are specialized regulatory pathways that allow bacteria to perceive their external environment and respond with various cellular behaviors (1–3). In these systems, environmental signals are transduced inside the cells initially by the aid of receptors also termed Methyl-accepting Chemotaxis Proteins (MCP). Most MCPs possess a transmembrane domain but 14% are soluble proteins (4). Ligand-bound MCPs regulate the autophosphorylation of the histidine kinase CheA that, in turn, transfers phosphoryl groups to at least two response regulators: CheY which is the most downstream component of the pathway and CheB which, together with CheR, constitutes the adaptation module. Che systems also include one or more of the docking protein CheW, interacting both with the C-terminal cytoplasmic tip of the MCP and with the P5 domain of CheA. CheW and $CheA^{P5}$ are paralogs and are topologically similar to SH3 domains from eukaryotic scaffold proteins that also play a role in signal transduction. Such domains are characterized by two intertwined 5-stranded β-strands designated subdomain 1 and 2 (5–7). MCP: $CheA^{P5}$: CheW interactions all involve subdomain 1 and 2. In particular, the β-strands 3 and 4 of subdomain 1 of $CheA^{P5}$ interacts with the β-strands 4 and 5 of subdomain 2 of CheW (8). The receptor cytoplasmic tip binds CheW or CheA at their hydrophobic junction between subdomain 1 and 2 (8).

High-resolution microscopy revealed that, intracellularly, Che proteins are organized in complex arrays running parallel to the bacterial inner membrane, with the MCP layer linked to a CheA/W baseplate (9, 10). Transversal views of these Che arrays show ordered MCP hexagons networked by CheA-CheW rings. CheA-CheW rings are composed of alternating and interacting $CheA^{P5}$ domains and CheWs. MCPs hexagons are constituted by six MCP trimers of dimers. Each MCP in the dimer is connected with either a $CheA^{P5}$ domain or a CheW, which allows connections between the MCP hexagons and the CheW-$CheA^{P5}$ rings

(11) (Fig. 1). The presence of each of these three proteins is essential for the integrity of the system (12, 13). This structure underlies the typical signaling properties of chemotaxis systems, including signal amplification and sensitivity (14–17).

The gliding bacterium *M. xanthus* uses the cytoplasmic Frz signal transduction pathway to bias the frequency at which bacteria change their movement direction in response to environmental signals (18). This chemotactic-like behavior might allow bacteria to glide towards favorable directions or away from toxic compounds. The Frz system induces a cell reversal by promoting the coordinate inversion of the cell polarity of the two *M. xanthus* motility systems: the Social (S) motility system powered by polar Type IV Pili and the Adventurous (A) motility powered by polarly assembled Agl-Glt complexes (19–21). The regulation of the motility systems by the Frz pathway is fundamental for cells to enter a developmental program that leads to the formation of multicellular fruiting bodies. The Frz core is composed of a cytoplasmic MCP (FrzCD), a CheA (FrzE) and a CheW (FrzA) (22). In the absence of any of these three proteins cells display drastically reduced reversal frequencies and are no longer able to respond to isoamyl alcohol (IAA), a Frz activator (20, 22). The Frz system also includes a second CheW-like protein, FrzB described as an accessory because while in its absence cells show phenotypes similar to those caused by the deletion of core proteins, *ΔfrzB* cells are still able to respond to IAA with increased reversal frequencies (20, 22).

In this paper, we show that FrzB is a divergent CheW lacking the β-strands involved in the interaction with the histidine kinase FrzE (β4 and β5). Strikingly, the introduction of β4 and β5 from FrzA to FrzB, converts the latter into a canonic CheW. Instead of mediating signal transduction from the FrzCD receptor to FrzE, FrzB acts upstream of FrzCD to allow the formation of multiple distributed Frz chemosensory arrays at the nucleoid, which in turn

allows cell reversals. These clusters collapse in a unique and less active array in the absence of FrzB. Finally, the loss of the CheA-interacting region in FrzB might have been selected to confer plasticity to nucleoid-associated chemosensory systems.

RESULTS

FrzB is upstream of the FrzCD receptor in the Frz signaling pathway

The first two genes of the *frz* operon encode the CheW-like proteins, FrzA and FrzB. *ΔfrzA* cells show the same motility and fruiting body formation phenotypes as *ΔfrzCD* and *ΔfrzE* suggesting that FrzA is the core CheW of the Frz pathway (22, 23) (Fig. 2A). The aberrant behaviors at the colony level are due to the inability of *ΔfrzA* to modulate single cell reversal frequencies even in the presence of isoamyl alcohol (IAA), a known Frz activator (Fig. 2B) (20, 22).

While a *frzB* deletion causes the same defects as *ΔfrzA* in the absence of IAA, IAA completely rescues the reversal frequency defect of *ΔfrzB* cells (Fig. 2B). This effect is detectable at both single cell and colony level (Fig. 2) (22). These results show that signals from the FrzCD receptor can still be transduced to FrzE in the absence of FrzB and, thus, FrzB is not part of the Frz core.

Then, in order to determine the functional position of FrzB in the Frz pathway, we tested the epistasis of FrzB in respect to FrzCD. Because FrzCD is a central component of the Frz pathway, *ΔfrzB ΔfrzCD* and *ΔfrzA ΔfrzCD* double mutants showed the same aberrant motility and developmental phenotypes as *ΔfrzCD* (and *ΔfrzA*) at both single cells and colony levels (Figure S1 and Fig. 2) (22). We, thus, took advantage of a *frzCD* allele, *frzCDc*, whose expression confers a constitutively hyper-reversing phenotype (Fig. 2) (Bustamante et al., 2004) and constructed *ΔfrzA frzCDc* and *ΔfrzB frzCDc* double mutants. The *ΔfrzA frzCDc* reversal frequencies and colony phenotypes were indistinguishable from those of *ΔfrzA* cells, confirming that FrzA is located downstream of the receptor in the signaling pathway (Fig. 2). On the other hand, *ΔfrzB frzCDc* phenotypes resembled those of *frzCDc* (Fig. 2) indicating

that FrzB is upstream of FrzCD in the Frz signaling pathway and that its requirement is bypassed by a constitutive *frzCDc* mutation.

FrzB does not interact with the downstream histidine kinase FrzE

Genetic data show that FrzB is upstream of FrzCD in the Frz regulatory pathway. We, thus, wanted to verify if FrzB could interact with FrzE. For this, we performed bacterial two-hybrid protein-protein interaction assays. As expected, both FrzA and FrzB interacted with FrzCD as well as with the FrzCD signaling domain alone ($FrzCD^{Cter}$). On the other hand, only FrzA but not FrzB interacted with the FrzE-P5 domain ($FrzE^{P5}$) (Fig. 3A). Neither FrzA nor FrzB could interact with the FrzCD nucleoid binding N-terminal domain (Fig. 3A).

If FrzB does not interact with FrzE, it should not be able to promote the phosphorylation of the FrzE kinase domain ($FrzE^{CheA}$) *in vitro*. In fact, it has been previously shown that the presence of both FrzCD and FrzA is strictly required to achieve the transfer of a phosphoryl group from ATP to the Histidine at position 49 of $FrzE^{CheA}$ *in vitro* (24) (Fig. 3B). As expected, when we replaced FrzA with FrzB in the mixture no phosphorylation was detected suggesting that FrzB cannot mediate the $FrzE^{CheA}$ autophosphorylation *in vitro* (Fig. 3B).

Next, we asked what prevented FrzB from interacting with FrzE. To address this question, we decided to generate 3D homology models of the $FrzE^{P4-P5}$:FrzA and $FrzE^{P4-P5}$:FrzB complexes based on the *T. maritima* $CheA^{P4-P5}$:CheW crystal structure (Fig. 3C) (8). The structural models predict that FrzB cannot interact with FrzE due to the lack of a 20 amino acid region forming the β-strands 4 and 5 of subdomain 2 and corresponding exactly to the CheW region important for the CheW: $CheA^{P5}$ interaction (Fig. 3C and D) (8). On the other hand, and consistently with the two-hybrid system results, FrzB is predicted to contain all the hydrophobic amino acids involved in its interaction with FrzCD (Fig. 3D).

To verify if the lack of the FrzE interacting region in FrzB was directly associated with the loss of the FrzB-FrzE interaction, we designed a chimeric FrzB protein carrying the β-strands 4 and 5 from FrzA ($FrzB^{\beta4-\beta5}$). First, we tested if purified $FrzB^{\beta4-\beta5}$ was able to replace FrzA in our $FrzE^{CheA}$ phosphorylation *in vitro* assay. Strikingly, when $FrzB^{\beta4-\beta5}$ was the only CheW in the reaction mixture, it promoted the $FrzE^{CheA}$ phosphorylation similarly to FrzA, thus acting as a CheW (Fig. 3B). The $FrzE^{CheA}$ phosphorylation levels were a direct consequence of the FrzCD activation state, because when we used the hyperactive $FrzCD^{c}$ allele in the place of its wild type version, we observed a higher level of phosphorylated $FrzE^{CheA}$ (Fig. 3B).

Then, to test whether $FrzB^{\beta4-\beta5}$ could replace FrzA *in vivo* as *in vitro*, we transferred the gene coding for $FrzB^{\beta4-\beta5}$ in a *ΔfrzA ΔfrzB* strain at the endogenous locus. $FrzB^{\beta4-\beta5}$ was stably expressed (Figure S2) and the resulting strain had phenotypes and reversal frequencies similar to those of *ΔfrzB* both in the presence and in the absence of IAA (Fig. 2). These results suggest that *in vivo,* like *in vitro*, $FrzB^{\beta4-\beta5}$ can connect FrzCD to FrzE, like FrzA. Surprisingly, a *ΔfrzA* $frzB^{\beta4-\beta5}$ strain phenocopied *ΔfrzA* and was, thus, more defective than *ΔfrzA ΔfrzB* $frzB^{\beta4-\beta5}$ (Figure S3). This result might be due to the fact that even if $FrzB^{\beta4-\beta5}$ is able to act as a CheW when expressed alone (like in *ΔfrzA ΔfrzB* $frzB^{\beta4-\beta5}$), $FrzB^{\beta4-\beta5}$ could interfere with FrzB when the two proteins are co-expressed. On the other hand, a *ΔfrzB* $frzB^{\beta4-\beta5}$ strain showed wild type phenotypes in the presence as in the absence of IAA, suggesting that $FrzB^{\beta4-\beta5}$ could fully replace FrzB if expressed together with FrzA (Figure S3).

FrzB might be a stabilizing factor of multiple Frz signaling arrays

It has been previously shown that Frz proteins form nucleoid associated signaling complexes (25, 26). To verify whether FrzB was part of the Frz clusters, we constructed a *mCherry-frzB* fusion that replaced *frzB* at the endogenous locus and encoded a functional protein (Figure

S2 and S4). MCherry-FrzB formed multiple-nucleoid associated clusters that resembled those formed by FrzCD-GFP and FrzE-mCherry (Fig. 4A) (26), suggesting that the three proteins are part of the same complexes.

Then, we decided to check how the absence of FrzA and FrzB affected the formation of these complexes. For that, we transferred a *frzCD-gfp* gene fusion (26) in the *ΔfrzA* and *ΔfrzB* mutants. *M. xanthus* cells of the resulting strains were then imaged by fluorescence microscopy. While FrzCD-GFP was completely dispersed in the cytoplasm in the absence of FrzA, this fusion protein formed a single nucleoid-associated cluster in the absence of FrzB (Fig. 4B), suggesting that even if FrzB is dispensable for the assembly of Frz chemosensory arrays, it is important for the formation of multiple distributed clusters on the nucleoid. These clusters collapse in a single cluster in the absence of FrzB. The aberrant localization patterns were not due to a change in the FrzCD-GFP protein levels (Figure S5). Interestingly, and by yet unknown mechanisms, FrzA not only is essential for Frz cluster formation, but it also allows the association of FrzCD to the nucleoid (Fig. 4).

DISCUSSION

Chemosensory systems are modified two component systems where the addition of accessory proteins confers unique properties like signal amplification and sensitivity. In this work, we found that the CheW-like protein FrzB lacks a 20 amino acid sequence corresponding to two β-strands that in chemosensory systems are important for CheA:CheW interactions (8). Thus, FrzB cannot interact with FrzE and mediate its autophosphorylation. The loss of this protein region might have been selected to confer to this small protein the unique function of allowing the formation and distribution of multiple nucleoid Frz chemosensory arrays. How would FrzB accomplish these tasks? It has been shown that Che arrays are constituted by hexagons of MCP trimers of dimers networked by Che^{P5}-CheW rings (11). However, if FrzB cannot interact with $FrzE^{P5}$, it cannot participate to the formation of Che^{P5}-CheW rings either. In addition to Che^{P5}-CheW rings, the formation of Che networks implies the formation of six-member CheW rings that only interact with the MCPs (Fig. 1) (17, 27, 28). The 6-CheW rings have been visualized by cryoEM and their suggested function is to stabilize the Che arrays. We can imagine that FrzB participates to the formation of this kind of rings to "destabilize" and confer plasticity to Frz arrays (Fig. 1).

Interestingly, the FrzCD receptor does not contain an obvious signal-binding domain. Instead, it contains an N-terminal region that has been recently shown to be involved in DNA binding (26). Thus, FrzB could also function to deliver signals to the Frz pathway. FrzB might bind directly some cytoplasmic molecules and transduce signals to FrzCD, thus, functioning as a sensor of the cellular metabolic state. However, FrzB could also connect FrzCD to another MCP or sensor kinase. *M. xanthus* encodes a total of 21 MCPs (30). Among them, only Mcp7 is cytoplasmic like FrzCD, but its localization strongly excludes an association with the Frz pathway (30). We could imagine that FrzCD, which forms clusters on the nucleoid

(25, 26), could associate with a transmembrane MCP or sensor kinase at regions where the nucleoid surface is particularly close to the inner membrane (31). In fact, previous works show the association of FrzCD with membrane fractions (32) as well as interactions with envelop-associated A-motility proteins (33, 34). The hypothesis that FrzB is a Frz input does not rule out that FrzCD itself can somehow bind signals. Indeed, FrzCD responds to IAA independently on FrzB (Fig. 2).

In the last years, the discovery of different accessories Che proteins allowed the identification of new functions and degrees of complexity in the regulation of the cellular responses operated by chemosensory systems. By unraveling a new accessory protein and its function, this work open new insights on the knowledge of the regulatory potentials of bacterial chemosensory systems.

EXPERIMENTAL PROCEDURES

Bacterial strains, plasmids and growth

*S*trains and plasmids are listed in Table S1 and S2, respectively. *M. xanthus* strains were grown at 32°C in CYE rich media as previously described.

Plasmids were introduced into *M. xanthus* cells by electroporation. Deletions and GFP fusions were inserted in frame, using the pBJ113 or pBJ114 vectors, to avoid polar effects on the downstream gene expression (22, 30).

Strains EM736 and EM743 were obtained by deleting *frzA* from codon 15 to 145 and *frzB* from codon 11 to 92, respectively. In both strains we also deleted *frzCD* from codon 6 to 182. Strain EM742 was obtained by deleting *frzA* and *frzB* as above.

To construct plasmid pEM399 to generate EM515, a DNA fragment was generated by PCR overlapping a DNA region amplified with primers CCCAAGCTTCTTCAGCTCGAGGCTGGCAA and TGCCCCTTGCTCACCATCTCCTCCTCCTTCTCATGGAA and *mCherry* amplified with primers CATGAGAAGGAGGAGGAGATGGTGAGCAAGGGCGAGGA and CGGGATCCTCTAGACTTGCACAGCTCGTCCATGC from pEM147 (33). This fusion product was digested with HindIII and BamHI. *frzB* was amplified with primers CGGGATCCGGAGCAGGAGACCTCCTCTTCTTCGACAT and GGAATTCGCGGACGAGGACAGCCTCAA and digested with BamHI and EcoRI. The two fragments were then cloned into pBJ113 previously digested with HindIII and BamHI in a three-partner ligation reaction.

To obtain strains EM440 and EM512, plasmid pDPA20 was transferred into strains DZ4479 and DZ4478 respectively.

For the construction of $frzB^{\beta4\text{-}\beta5}$ we replaced codon 27 to 36 of FrzB with codon 41 to 75 of FrzA. Plasmids pEM463 was synthesized by Biomatik.

To construct the plasmids used in the two hybrid-system assays, we PCR amplified the DNA coding sequences of interest (Table 2) without the ATG; digested them with XbaI and EcoRI and cloned them into pKT25 and pUT18C (Euromedex) previously digested with the same enzymes. $FrzCD^{Cter}$ and $FrzCD^{Nter}$ (Table 2) were chosen based on previous works (22, 35). To construct pEM391 and pEM392, *frzB* without the ATG was amplified, digested with HindIII and XbaI and cloned into pKTN25 and pUT18 (Euromedex), respectively, previously digested with the same enzymes.

Escherichia coli cells were grown under standard laboratory conditions in LB broth supplemented with antibiotics if necessary.

For swarming and fruiting body assays, cells (5 µl) at a concentration of 5×10^{9} cfu ml^{-1} were spotted on CYE or CF (for fruiting body formation) agar plates and incubated at 32°C and photographed after respectively 48h or 72h with an Olympus SZ61 binocular stereoscope.

Reversal frequencies

5 µl of cells from 4 x 10^{8} cfu ml^{-1} vegetative CYE cultures were spotted on a thin fresh TPM agar supplied or not with 0.15 % IAA. Time-lapse movies were shot for 1 hour with frames captured every 30 seconds. Movies were obtained and reversal frequencies calculated with Image J (Rasband, W.S., ImageJ, U. S. National Institutes of Health, Bethesda, Maryland, USA, http://imagej.nih.gov/ij/, 1997-2012) and FIJI as previously described (20). For non-reversing strains, the number of reversals for each cell was plotted against time using the R software (https://www.r-project.org/). For strain that frequently reverse, the number of periods between two reversals are plotted against time using the R software. Reversal frequencies were measured from cells issued from two to six biological replicates. Statistical significance was obtained with a Wilcox Test from R.

1

2 **Bacterial two-hybrid experiments**

3 Bacterial two-hybrid experiments were performed on plates as previously described (30) and

4 as recommended by the manufacturer instructions (Euromedex).

5

6 **Sequence alignment and homology modeling**

7 Predictions of secondary structures and protein sequence alignments were obtained with

8 Jpred (36) and Clustal Omega (37), respectively. Homology models of FrzA (Uniprot P43498)

9 or FrzB (Uniprot P43499) in the presence of FrzE (Uniprot P18769) were built with

10 MODELLER 9v12 (38). Crystal structure of the complex between bacterial chemotaxis

11 histidine kinase $CheA^{P4-P5}$ and receptor-adaptor protein CheW (PDB codes 2CH4) was used as

12 template (39). The modeling was performed in a two-step manner: First, each individual

13 domain was modeled separately using the 3D structure of its *T. maritima* counterpart as a

14 template. CheW (2CH4 chain W) was used to build models of FrzA and FrzB. The N terminal

15 domain of CheA (2CH4 chain A resid 355-540) and the C terminal domain of CheA (2CH4

16 chain A resid 541-671) were used to build N and C terminal domains of FrzE. In a second

17 step, each model was superimposed to its counterpart in the x-ray structure of the CheW-

18 CheA complex (chains W and A). The Frz proteins exhibit high enough identities to their Che

19 counterparts to build reasonable 3D models. FrzB vs CheW (26.1% identity, 45% similarity),

20 FrzA vs CheW (26.6% identity, 46.7% similarity), $FrzE^{p4}$ vs. $CheA^{p4}$ (46.5% identity, 71.7%

21 similarity), $FrzE^{p5}$ vs. $CheA^{p5}$ (26.1% identity, 53.8% similarity). Quality of the models was

22 assessed with Prosess server (http://www.prosess.ca). Structural alignments were

23 performed with Protein structure comparison service PDBeFold at European Bioinformatics

24 Institute (http://www.ebi.ac.uk/msd-srv/ssm) (40). Fig. 3C showing the lowest energy model

was generated with pymol (http://pymol.org). Fig. 3D was generated with ESPript web server (41).

Fluorescence microscopy and image analysis

For fluorescence microscopy analyses, 5 ml of cells from 4 x 10^8 cfu ml^{-1} vegetative CYE cultures were spotted on a thin fresh TPM agar pad at the top a slide (42). A cover slip was added immediately on the top of the pad, and the obtained slide was analyzed by microscopy using a Nikon Eclipse TE2000 E PFS inverted epifluorescence microscope (100 x oil objective NA 1.3 Phase Contrast) (43).

To study the colocalization with the DNA, the TPM agar pads were supplied with 1µg ml^{-1} DAPI stain as shown by Moine et al. (26). FrzB clusters, nucleoid areas and cell areas were automatically detected and verified manually with the "MicrobeJ" Fiji/ImageJ plugin created by A. Ducret, Brun Lab (http://www.indiana.edu/~microbej/index.html). All data plots and statistical tests were obtained with the R software (https://www.r-project.org/).

***In vitro* autophosphorylation assay**

In vitro phosphorylation assays were performed with *E. coli* purified recombinant proteins. 4 µg of $FrzE^{CheA}$ were incubated with 1 µg of FrzA, FrzB or $FrzB^{\beta4\text{-}\beta5}$ and FrzCD or $FrzCD^{c}$ in 25 µl of buffer P (50 mM Tris-HCl, pH 7.5; 1 mM DTT; 5 mM $MgCl_2$; 50 mM KCl; 5 mM EDTA; 50 µM ATP, 10% (v/v) glycerol) supplemented with 200 µCi ml^{-1} (65 nM) of [γ-33P]ATP (PerkinElmer, 3000 Ci $mmol^{-1}$) for 10 minutes at room temperature in order to obtain the optimal $FrzE^{CheA}$ autophosphorylation activity. Each reaction mixture was stopped by addition of 5 × Laemmli and quickly loaded onto SDS-PAGE gel. After electrophoresis, proteins were

revealed using Coomassie Brilliant Blue before gel drying. Radioactive proteins were visualized by autoradiography using direct exposure to film (Carestream).

Acknowledgements

Research on chemotaxis in our laboratory is funded by the Agence National de la Recherche Jeune Chercheur-Jeune Chercheuse (ANR-14-CE11-0023-01) to E.M.M.

The authors have no conflicts of interest to declare.

References

1. Sourjik V, Berg HC (2002) Binding of the Escherichia coli response regulator CheY to its target measured in vivo by fluorescence resonance energy transfer. *Proc Natl Acad Sci U S A* 99(20):12669–12674.

2. Berleman JE, Bauer CE (2005) Involvement of a Che-like signal transduction cascade in regulating cyst cell development in Rhodospirillum centenum. *Mol Microbiol* 56(6):1457–1466.

3. Bible A, Russell MH, Alexandre G (2012) The Azospirillum brasilense Che1 chemotaxis pathway controls swimming velocity, which affects transient cell-to-cell clumping. *J Bacteriol* 194(13):3343–3355.

4. Collins KD, Lacal J, Ottemann KM (2014) Internal sense of direction: sensing and signaling from cytoplasmic chemoreceptors. *Microbiol Mol Biol Rev MMBR* 78(4):672–684.

5. Bilwes AM, Alex LA, Crane BR, Simon MI (1999) Structure of CheA, a signal-transducing histidine kinase. *Cell* 96(1):131–141.

6. Griswold IJ, et al. (2002) The solution structure and interactions of CheW from Thermotoga maritima. *Nat Struct Biol* 9(2):121–125.

7. Reebye V, et al. (2012) A perspective on non-catalytic Src homology (SH) adaptor signalling proteins. *Cell Signal* 24(2):388–392.

8. Li X, et al. (2013) The 3.2 Å resolution structure of a receptor: CheA:CheW signaling complex defines overlapping binding sites and key residue interactions within bacterial chemosensory arrays. *Biochemistry (Mosc)* 52(22):3852–3865.

9. Khursigara CM, Wu X, Subramaniam S (2008) Chemoreceptors in Caulobacter crescentus: trimers of receptor dimers in a partially ordered hexagonally packed array. *J Bacteriol* 190(20):6805–6810.

10. Briegel A, et al. (2009) Universal architecture of bacterial chemoreceptor arrays. *Proc Natl Acad Sci U S A* 106(40):17181–17186.

11. Briegel A, et al. (2012) Bacterial chemoreceptor arrays are hexagonally packed trimers of receptor dimers networked by rings of kinase and coupling proteins. *Proc Natl Acad Sci U S A* 109(10):3766–3771.

12. Sourjik V, Berg HC (2000) Localization of components of the chemotaxis machinery of Escherichia coli using fluorescent protein fusions. *Mol Microbiol* 37(4):740–751.

13. Wadhams GH, Martin AC, Warren AV, Armitage JP (2005) Requirements for chemotaxis protein localization in Rhodobacter sphaeroides. *Mol Microbiol* 58(3):895–902.

14. Sourjik V, Berg HC (2004) Functional interactions between receptors in bacterial chemotaxis. *Nature* 428(6981):437–441.

15. Ames P, Parkinson JS (2006) Conformational suppression of inter-receptor signaling defects. *Proc Natl Acad Sci U S A* 103(24):9292–9297.

16. Li M, Hazelbauer GL (2014) Selective allosteric coupling in core chemotaxis signaling complexes. *Proc Natl Acad Sci U S A* 111(45):15940–15945.

17. Piñas GE, Frank V, Vaknin A, Parkinson JS (2016) The source of high signal cooperativity in bacterial chemosensory arrays. *Proc Natl Acad Sci U S A* 113(12):3335–3340.

18. Blackhart BD, Zusman DR (1985) "Frizzy" genes of Myxococcus xanthus are involved in control of frequency of reversal of gliding motility. *Proc Natl Acad Sci U S A* 82(24):8767–8770.

19. Treuner-Lange A, et al. (2015) The small G-protein MglA connects to the MreB actin cytoskeleton at bacterial focal adhesions. *J Cell Biol* 210(2):243–256.

20. Guzzo M, et al. (2015) Evolution and Design Governing Signal Precision and Amplification in a Bacterial Chemosensory Pathway. *PLoS Genet* 11(8):e1005460.

21. Chang Y-W, et al. (2016) Architecture of the type IVa pilus machine. *Science* 351(6278):aad2001.

22. Bustamante VH, Martinez-Flores I, Vlamakis HC, Zusman DR (2004) Analysis of the Frz signal transduction system of Myxococcus xanthus shows the importance of the conserved C-terminal region of the cytoplasmic chemoreceptor FrzCD in sensing signals. *Mol Microbiol* 53(5):1501–13.

23. McBride MJ, Weinberg RA, Zusman DR (1989) "Frizzy" aggregation genes of the gliding bacterium Myxococcus xanthus show sequence similarities to the chemotaxis genes of enteric bacteria. *Proc Natl Acad Sci U S A* 86(2):424–428.

24. Inclán YF, Vlamakis HC, Zusman DR (2007) FrzZ, a dual CheY-like response regulator, functions as an output for the Frz chemosensory pathway of Myxococcus xanthus. *Mol Microbiol* 65(1):90–102.

25. Kaimer C, Zusman DR (2016) Regulation of cell reversal frequency in Myxococcus xanthus requires the balanced activity of CheY-like domains in FrzE and FrzZ. *Mol Microbiol* 100(2):379–395.

26. Moine A, et al. (2017) The nucleoid as a scaffold for the assembly of bacterial signaling complexes. *bioRxiv*:169912.

27. Liu J, et al. (2012) Molecular architecture of chemoreceptor arrays revealed by cryoelectron tomography of Escherichia coli minicells. *Proc Natl Acad Sci U S A* 109(23):E1481–1488.

28. Cassidy CK, et al. (2015) CryoEM and computer simulations reveal a novel kinase conformational switch in bacterial chemotaxis signaling. *Elife* 4. doi:10.7554/eLife.08419.

29. Briegel A, et al. (2016) Chemotaxis cluster 1 proteins form cytoplasmic arrays in Vibrio cholerae and are stabilized by a double signaling domain receptor DosM. *Proc Natl Acad Sci U S A* 113(37):10412–10417.

30. Moine A, et al. (2014) Functional organization of a multimodular bacterial chemosensory apparatus. *PLoS Genet* 10(3):e1004164.

31. Adams DW, Wu LJ, Errington J (2015) Nucleoid occlusion protein Noc recruits DNA to the bacterial cell membrane. *EMBO J* 34(4):491–501.

32. McBride MJ, Köhler T, Zusman DR (1992) Methylation of FrzCD, a methyl-accepting taxis protein of Myxococcus xanthus, is correlated with factors affecting cell behavior. *J Bacteriol* 174(13):4246–4257.

33. Mauriello EMF, Nan B, Zusman DR (2009) AglZ regulates adventurous (A-) motility in Myxococcus xanthus through its interaction with the cytoplasmic receptor, FrzCD. *Mol Microbiol* 72(4):964–977.

34. Nan B, Mauriello EMF, Sun I-H, Wong A, Zusman DR (2010) A multi-protein complex from Myxococcus xanthus required for bacterial gliding motility. *Mol Microbiol* 76(6):1539–1554.

35. Moine A, et al. (2017) The nucleoid as a scaffold for the assembly of bacterial signaling complexes. *PLoS Genet* 13(11):e1007103.

36. Cole C, Barber JD, Barton GJ (2008) The Jpred 3 secondary structure prediction server. *Nucleic Acids Res* 36(suppl 2):W197–W201.

37. Sievers F, Higgins DG (2014) Clustal omega. *Curr Protoc Bioinforma Ed Board Andreas Baxevanis Al* 48:3.13.1–16.

38. Webb B, Sali A (2016) Comparative Protein Structure Modeling Using MODELLER. *Curr Protoc Bioinforma Ed Board Andreas Baxevanis Al* 54:5.6.1–5.6.37.

39. Park S-Y, et al. (2006) Reconstruction of the chemotaxis receptor-kinase assembly. *Nat Struct Mol Biol* 13(5):400–407.

40. Krissinel E, Henrick K (2004) Secondary-structure matching (SSM), a new tool for fast protein structure alignment in three dimensions. *Acta Crystallogr D Biol Crystallogr* 60(Pt 12 Pt 1):2256–2268.

41. Gouet P, Robert X, Courcelle E (2003) ESPript/ENDscript: extracting and rendering sequence and 3D information from atomic structures of proteins. *Nucleic Acids Res* 31(13):3320–3323.

42. Mignot T, Merlie JP, Zusman DR (2005) Regulated pole-to-pole oscillations of a bacterial gliding motility protein. *Science* 310(5749):855–7.

43. Ducret A, et al. (2009) A microscope automated fluidic system to study bacterial processes in real time. *PLoS ONE* 4(9):e7282.

1

2

FIGURE LEGEND

Fig. 1. MCP form trimers of dimers (each dimer is shown as a green circle), which, in turn, form hexagons connected with rings composed of the CheA-P5 domain (dark blue bars) and CheW (white bars). A signaling unit is represented in the red box. The blue circles represent CheA-P4 domains. 6CheW-rings (shown at the center of the array) might serve to modulate the system stability and thus activation.

Fig. 2. FrzB is not required for the IAA response and is upstream to FrzCD. (A) Motility and fruiting body formation phenotypes were photographed at 48h and 72h, respectively. (B) Box plots of reversal frequencies of single cells moving on agar pads supplemented or not with 0,15% IAA. The lower and upper boundaries of the boxes correspond to 25% and 75% percentiles, respectively. The median is shown as a line at the center of each box and whiskers represents the 10% and 90% percentiles. For the reversal frequency measurements, approximately 500 cells, issued from three to six biological replicates, were used. *frzCDc* corresponds to the allelic variant *frzCDΔ6-182*.

Fig. 3. FrzB interacts with FrzCD but not with FrzE. (A) Bacterial two-hybrid assays on plates. Interactions between the indicated Frz proteins are shown: (+) indicates bacterial colonies turning red within 24h or 48h; (-) means that the colony color was as the negative control; ND stands for "not determined". We only show interactions reproducible in a biological replicate where each experiment was performed in triplicate. Examples of colonies from negative control (empty plasmids) and (pKT25C*mcpM*/pUT18C*cheW4b* from Moine *et al.*, 2014) are shown. (B) The $FrzB^{\beta4\text{-}\beta5}$ chimera can promote FrzE phosphorylation. The FrzE kinase domain ($FrzE^{CheA}$) auto-phosphorylation were tested *in vitro* by incubation of

1 $FrzE^{CheA}$ in the presence of FrzA, FrzB or $FrzB^{\beta4-\beta5}$, the indicated different forms of FrzCD and
2 $ATP\gamma P^{33}$ as a phosphate donor. (C) 3D models of the $FrzE^{P4-P5}$:FrzA and $FrzE^{P4-P5}$:FrzB
3 complexes based on the *T. maritima* $CheA^{P4-P5}$:CheW crystal structure (PDB 2ch4). The 20
4 amino acid region forming theβ-strands 4 and 5 of subdomain 2 and corresponding to the
5 CheW region important for the CheW:$CheA^{P5}$ interaction are highlighted in red in the FrzA
6 structure. These residues are missing in FrzB. (D) Protein structural alignments between *T.*
7 *maritima* CheW x-ray structure and *M. xanthus* FrzA and FrzB theoretical 3D models. CheW
8 residues in atomic contact with CheA and MCP are shown as red stars and blue squares
9 respectively. Secondary structures determined from CheW x-ray structure are shown on top
10 of the alignment.
11
12 **Fig. 4.** FrzB-mcherry colocalizes with the nucleoid in *M. xanthus*. (A) (Left) Micrographs of
13 *mcherry-frzB* cells stained with the DNA DAPI stain. (Middle) mCherry (red) and DAPI
14 fluorescence (blue) profiles are shown with the fluorescence intensity (arbitrary units)
15 represented on the *y*-axis and the cell length positions with -1 and +1 indicating the poles,
16 on the *x*-axis. The cell boundaries were drawn manually from the phase contrast images.
17 (Right) Correlation coefficients between the DAPI and mCherry localization are plot. R^2
18 values > 0,5 indicate significant correlations. The table compares the R^2 values between the
19 indicated fluorescent fusion and DAPI staining. (B) (Left) Fluorescence micrographs of the
20 indicated *M. xanthus* strains carrying a FrzCD-gfp fusions. The cell boundaries were drawn
21 manually from the phase contrast images. (Right) For each indicated strain, more than 120
22 cells (*x* axis) from biological replicates, are ordered according to their cell length (pixels) and
23 for each cell the GFP fluorescence intensity, along the cell body (from -1 to +1 on the *y* axis).

is represented as colored pixels at the corresponding cell position. “0” is the cell center. On the right, a scale indicates the fluorescent intensity and the corresponding colors.

1 **Table S1. Strain list**
2

Strains	Genotype	Reference or source
DZ2	*wt*	Zusman et al., 1982
DZ4478	*ΔfrzA*	Bustamante et al ; 2004
DZ4479	*ΔfrzB*	Bustamante et al ; 2004
DZ4487	*frzCDΔ6-182*	Bustamante et al ; 2004
DZ4480	*ΔfrzCD*	Bustamante et al ; 2004
EM538	*ΔfrzA frzCDΔ6-182*	This study
EM539	*ΔfrzB frzCDΔ6-182*	This study
DZ4620	*frzCD-gfp*	Mauriello et al., 2009
EM440	*ΔfrzB frzCD-gfp*	This study
EM512	*ΔfrzA frzCD-gfp*	This study
EM515	*frzB-mCherry*	This study
EM605	*ΔfrzA ΔfrzB frzB*$^{\beta4\text{-}\beta5}$	This study
EM736	*ΔfrzA ΔfrzCD*	This study
EM742	*ΔfrzA ΔfrzB*	This study
EM743	*ΔfrzB ΔfrzCD*	This study
EM699	*ΔfrzB frzB*$^{\beta4\text{-}\beta5}$	This study
EM700	*ΔfrzA frzB*$^{\beta4\text{-}\beta5}$	This study

3
4 **Table S2. Plasmid list**
5

Plasmid	Expression plasmid	Source
pEM411	pBJ113 with construct for *ΔfrzA frzCDΔ6-182*	This study
pEM412	pBJ113 with construct for *ΔfrzB frzCDΔ6-182*	This study
pEM463	pBJ113 with construct *ΔfrzA ΔfrzB frzB*$^{\beta4\text{-}\beta5}$ (Biomatik)	This study
pEM524	pBJ114 with construct *ΔfrzA ΔfrzB*	This study
pEM525	pBJ114 with construct *ΔfrzA* in DZ4480	This study
pEM526	pBJ114 with construct *ΔfrzB ΔfrzCD*	This study
pEM536	pBJ114 with construct *ΔfrzA frzB*$^{\beta4\text{-}\beta5}$	
pEM537	pBJ114 with construct *ΔfrzB frzB*$^{\beta4\text{-}\beta5}$	
pDPA20	pKY480 with construct for *frzCD-gfp*	Mauriello et al., 2009
pEM399	pBJ113 with construct for *frzB-mCherry*	This study
pEM443	pKT25 with *frzA*	This study
pEM391	pKTN25 with *frzB*	This study
pEM369	pKT25 with *frzCDΔ6-130*	This study
pEM370	pKT25 with *frzCDΔ143-417*	This study
pEM371	pKT25 with *frzCD*	This study
pEM372	pKT25 with *frzEΔ1-511/646-777*	This study
pEM379	pUT18C *frzA*	This study
pEM392	pUT18 *frzB*	This study
pEM381	pUT18C with *frzCDΔ6-130*	This study
pEM382	pUT18C with *frzCDΔ143-417*	This study
pEM382	pUT18C with *frzCD*	This study
pEM382	pUT18C with *frzEΔ1-511/646-777*	This study
pETPhos *frzCD*	pETPhos with *frzCD* tagged with 6-his inducible with IPTG	Guzzo et al., 2015
pETPhos *frzE*^{P5}	pETPhos with *frzE*^{kinase} tagged with 6-his inducible with IPTG	Guzzo et al., 2015
pETPhos *frzCD*^{c}	pETPhos with *frzCD*^{c} tagged with 6-his inducible with IPTG	Guzzo et al., 2015
pGEX(M) *frzA*	pETPhos with *frzA* tagged with 6-his inducible with IPTG	Guzzo et al., 2015
pETPhos *frzB*	pETPhos with *frzB* tagged with 6-his inducible with IPTG	This study
pEM464	pETPhos with *frzB*$^{\beta4\text{-}\beta5}$ tagged with 6-his inducible with IPTG (Biomatik)	This study
	pKT25	Euromedex
	pKTN25	Euromedex
	pUT18C	Euromedex
	pUT18	Euromedex

1 **SUPPLEMENTARY FIGURE LEGEND**

2 **Figure S1.** (A) Motility and fruiting body formation phenotypes were photographed at 48h
3 and 72h, respectively. (B) Box plots of reversal frequencies of single cells moving on agar
4 pads supplemented or not with 0,15% IAA. The lower and upper boundaries of the boxes
5 correspond to 25% and 75% percentiles, respectively. The median is shown as a line at the
6 center of each box and whiskers represents the 10% and 90% percentiles. For the reversal
7 frequency measurements, approximately 120 cells, issued from two biological replicates,
8 were used. For WT approximately 500 cells, issued from six biological replicates, were used.

9

10 **Figure S2.** Western blot with anti-FrzB antibodies on the cell extracts of the indicated *M.*
11 *xanthus* strains. The *pilA::frzB* strain, used as positive control, expresses *frzB* under the
12 control of the *pilA* promoter for high expression. The white line is used to indicate that two
13 lanes from the same gel were separated by other lanes in the original gel.

14

15 **Figure S3.** Motility and fruiting body formation phenotypes of the indicated strains were
16 photographed at 48h and 72h, respectively.

17

18 **Figure S4.** Motility and fruiting body formation phenotypes of the indicated strains were
19 photographed at 48h and 72h, respectively.

20

21 **Figure S5.** Western blot with anti-FrzCD antibodies on the cell extracts of the indicated *M.*
22 *xanthus* strains.

23

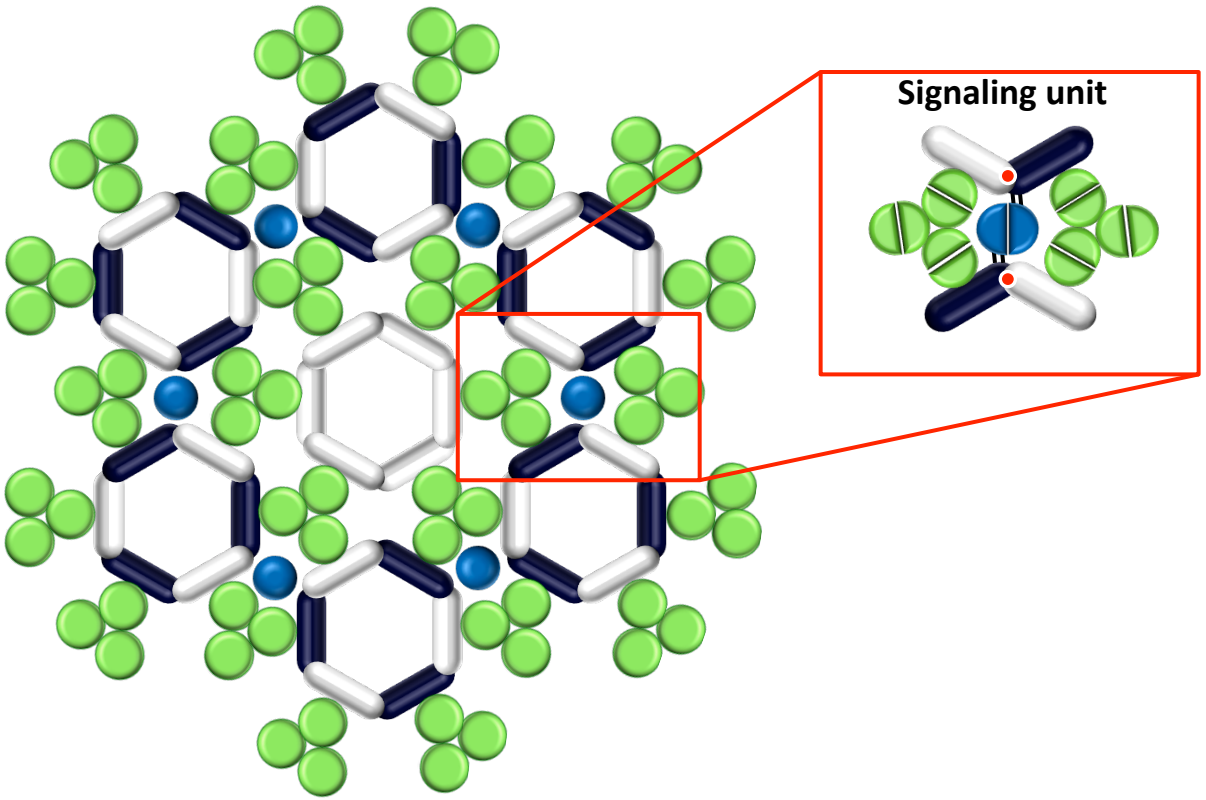
Signaling unit

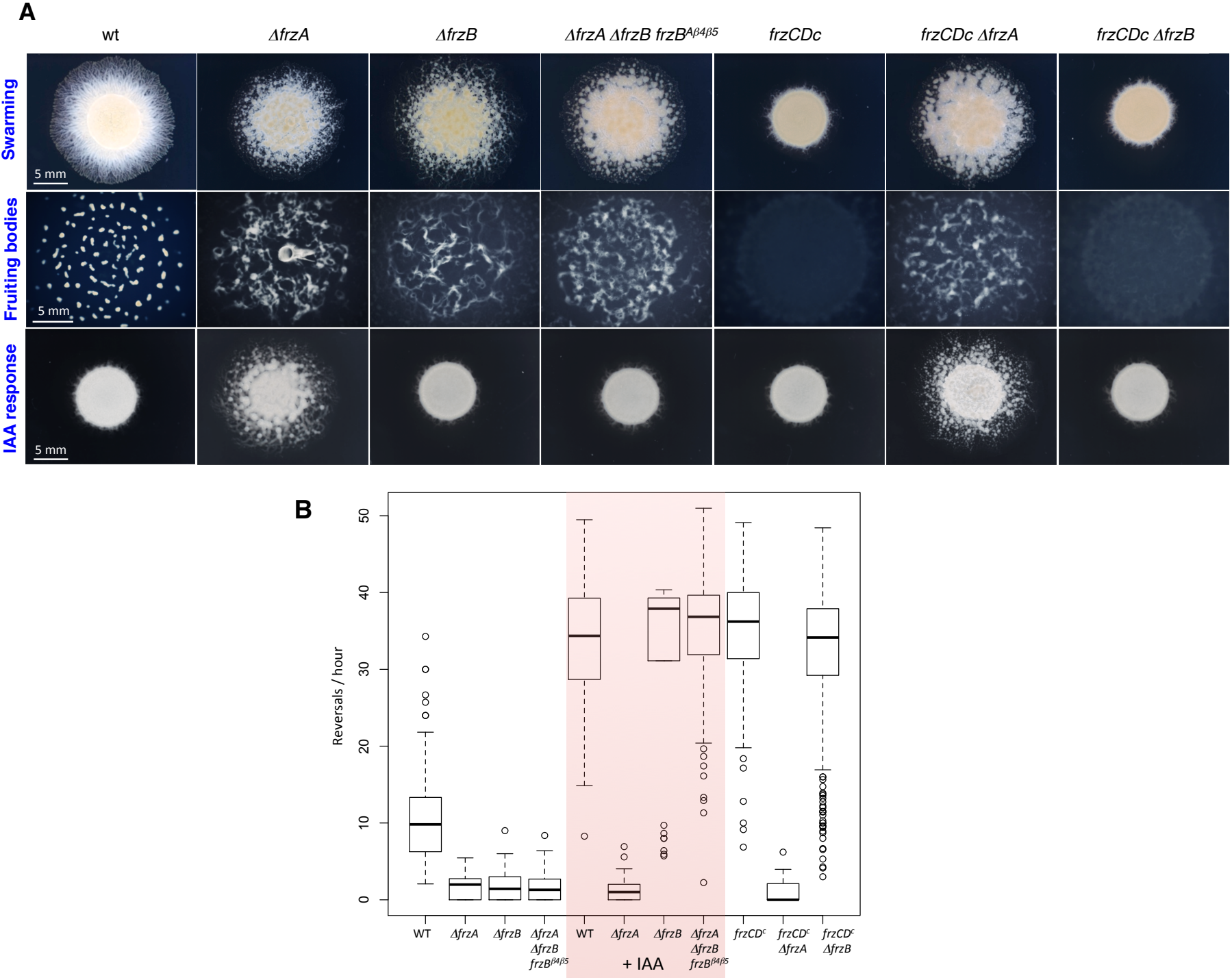
A
wt
ΔfrzA
ΔfrzB
ΔfrzA ΔfrzB frzB^Aβ4β5
frzCDc
frzCDc ΔfrzA
frzCDc ΔfrzB
Swarming
Fruiting bodies
IAA response
5 mm
B
Reversals / hour
0
10
20
30
40
50
WT
ΔfrzA
ΔfrzB
ΔfrzA ΔfrzB frzB^β4β5
WT
ΔfrzA
ΔfrzB
ΔfrzA ΔfrzB frzB^β4β5
frzCD^c
frzCD^c ΔfrzA
frzCD^c ΔfrzB
+ IAA

A

pUT18C / pKT25	FrzA	FrzB*	FrzCD	FrzCD^Cter	FrzCD^Nter	FrzE^P5
FrzA	ND	ND	+	+	-	+
FrzB**	ND	ND	+	+	-	-
FrzCD	+	+	ND	ND	ND	ND
FrzCD^Cter	+	+	ND	ND	ND	ND
FrzCD^Nter	-	-	ND	ND	ND	ND
FrzE^P5	+	-	ND	ND	ND	ND

* in pUT18, ** in pKTN25

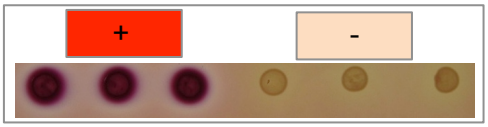

B

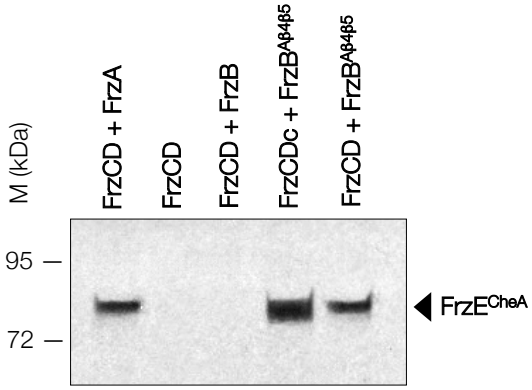

C

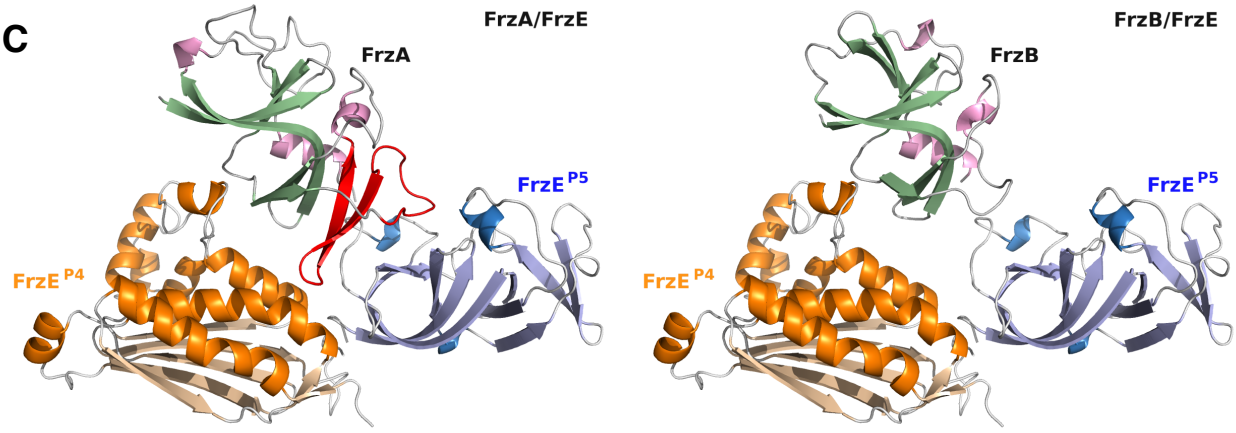

D

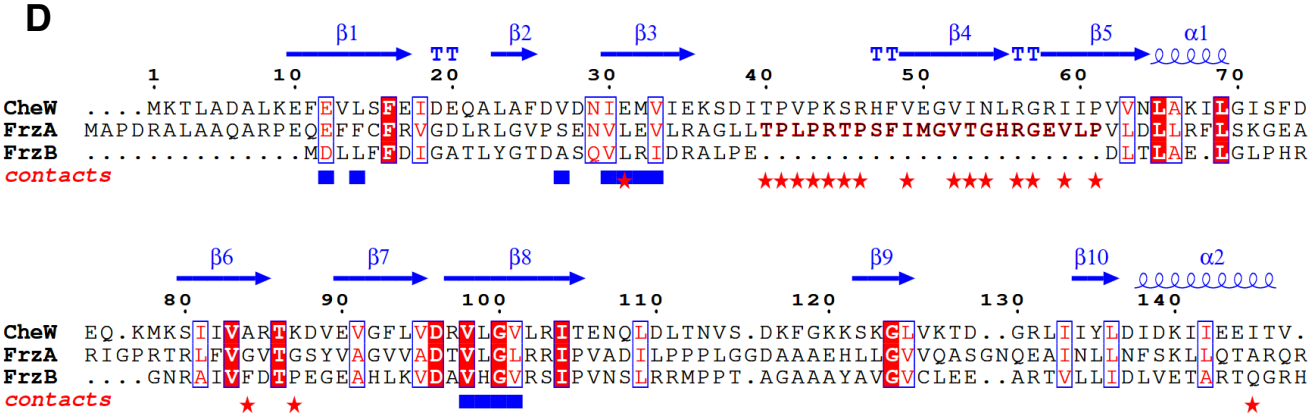

A

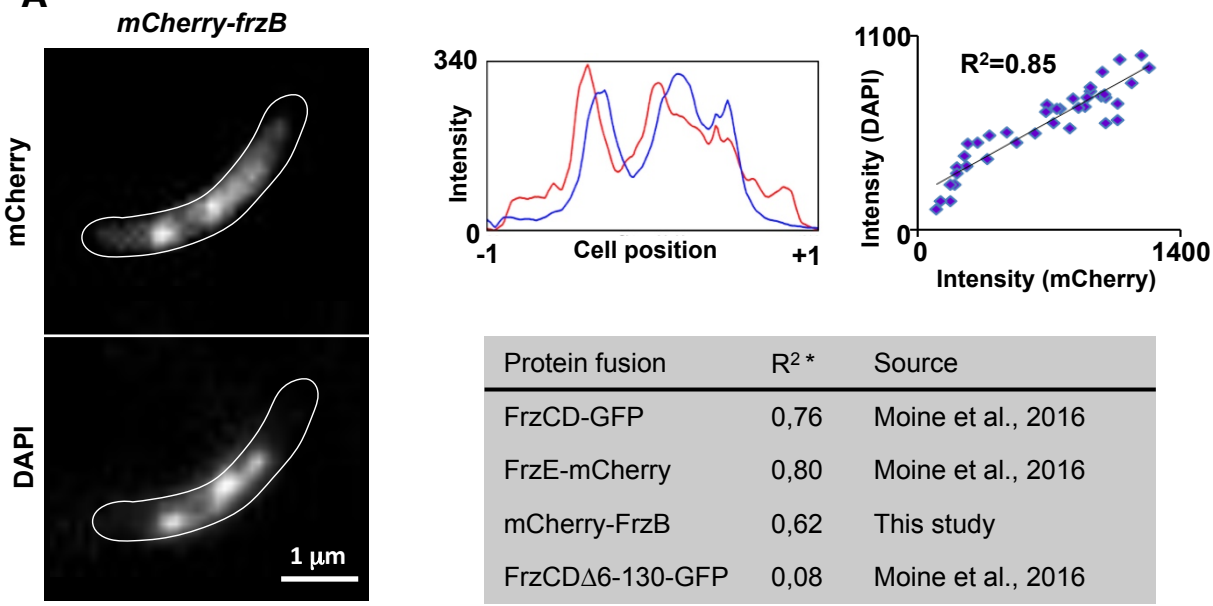

Protein fusion	R^2 *	Source
FrzCD-GFP	0,76	Moine et al., 2016
FrzE-mCherry	0,80	Moine et al., 2016
mCherry-FrzB	0,62	This study
FrzCD∆6-130-GFP	0,08	Moine et al., 2016

* Average of 10 cells

B

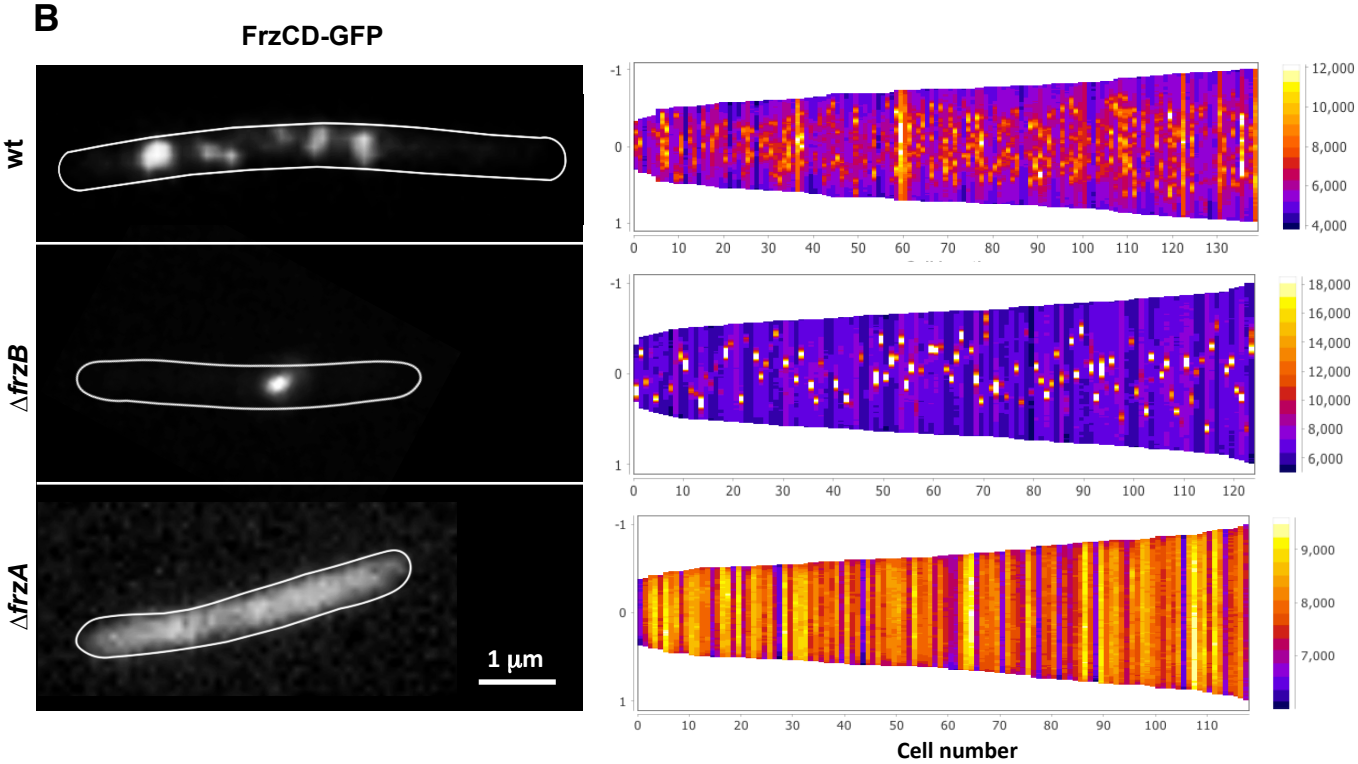

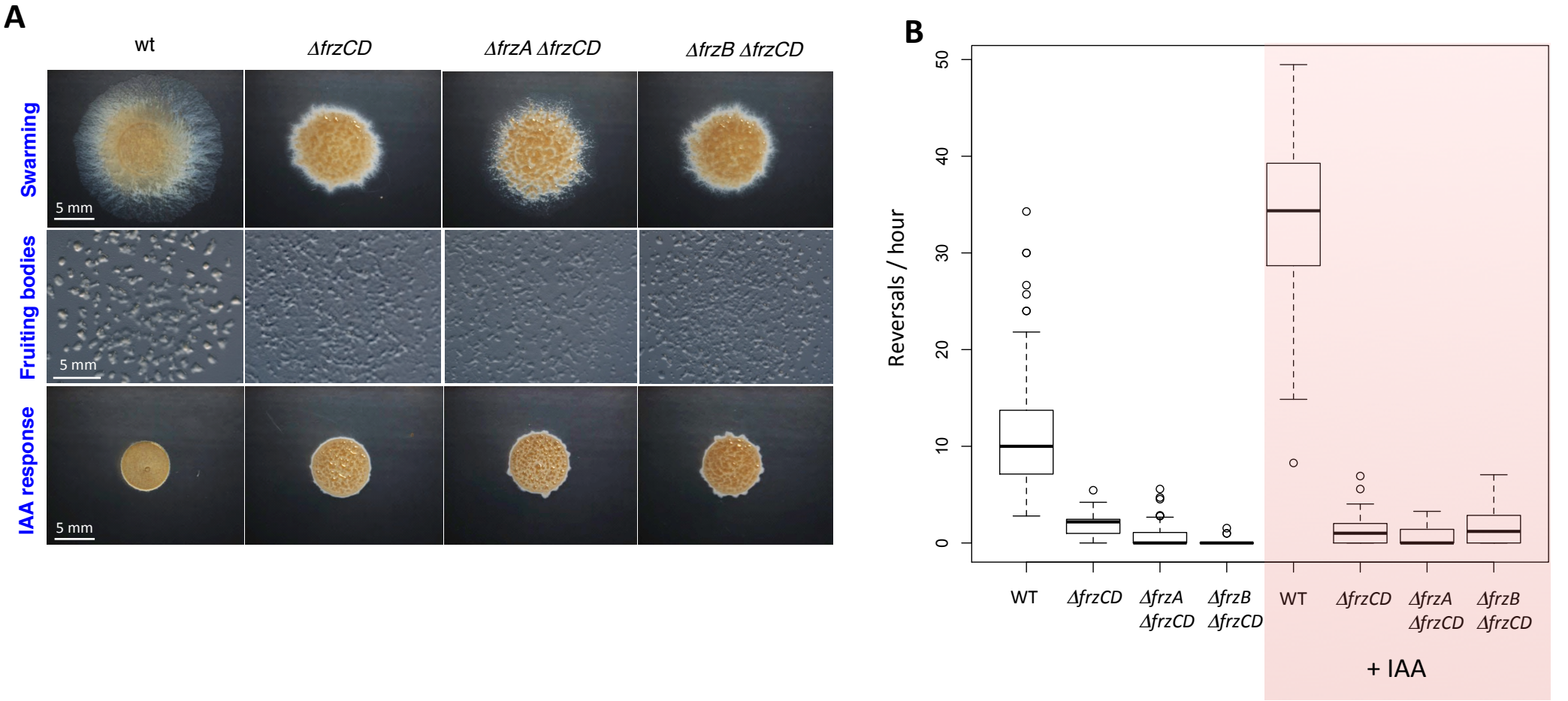
A
wt
ΔfrzCD
ΔfrzA ΔfrzCD
ΔfrzB ΔfrzCD
Swarming
Fruiting bodies
IAA response
5 mm
5 mm
5 mm
B
Reversals / hour
0
10
20
30
40
50
WT
ΔfrzCD
ΔfrzA ΔfrzCD
ΔfrzB ΔfrzCD
WT
ΔfrzCD
ΔfrzA ΔfrzCD
ΔfrzB ΔfrzCD
+ IAA

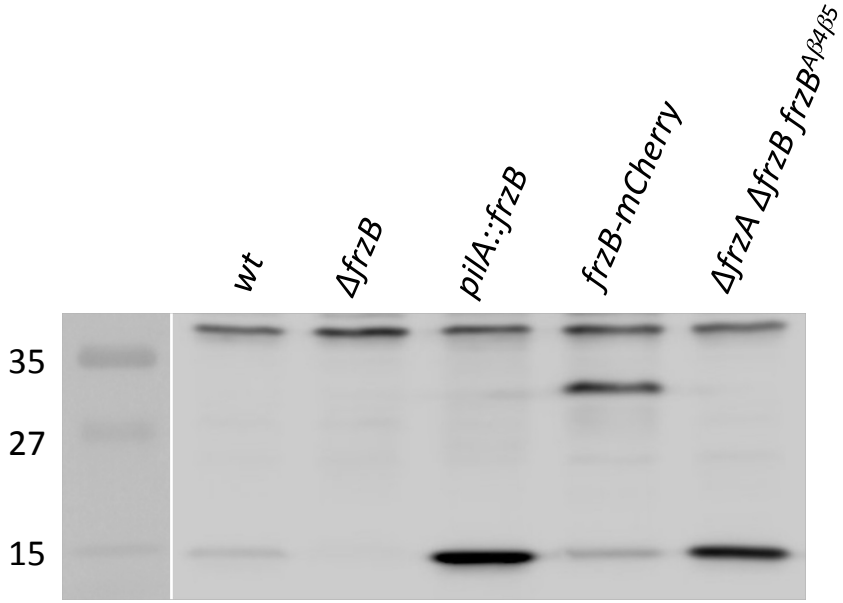
wt
ΔfrzB
pilA::frzB
frzB-mCherry
ΔfrzA ΔfrzB frzB$^{A\beta4\beta5}$
35
27
15

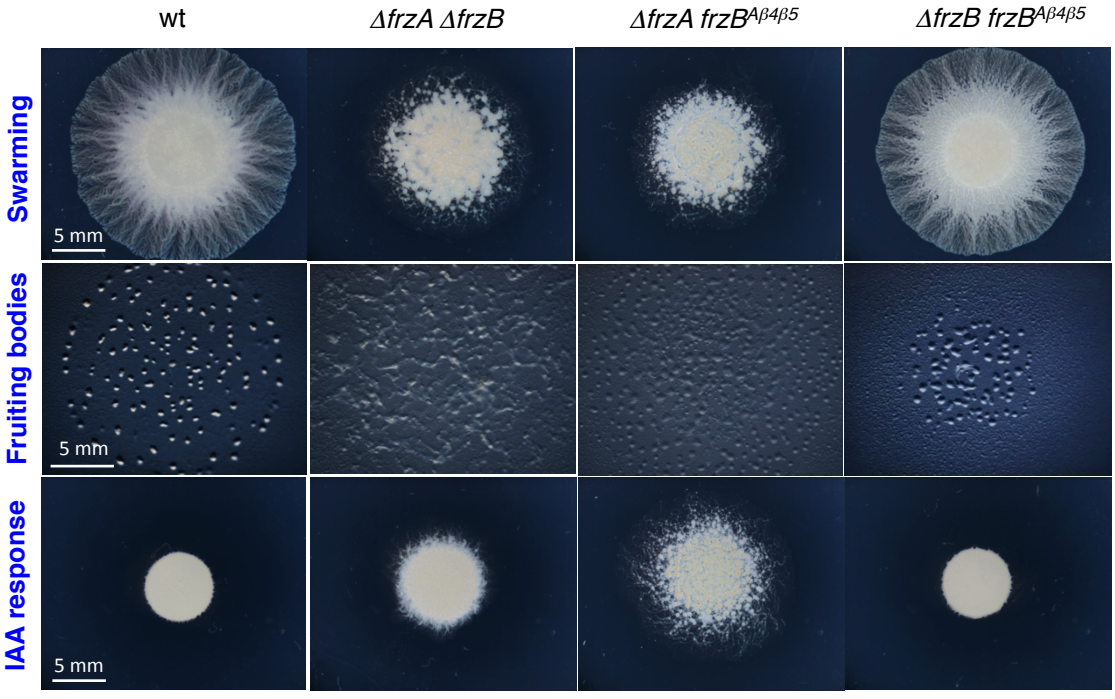
wt
ΔfrzA ΔfrzB
ΔfrzA frzB^Aβ4β5
ΔfrzB frzB^Aβ4β5
Swarming
Fruiting bodies
IAA response
5 mm
5 mm
5 mm

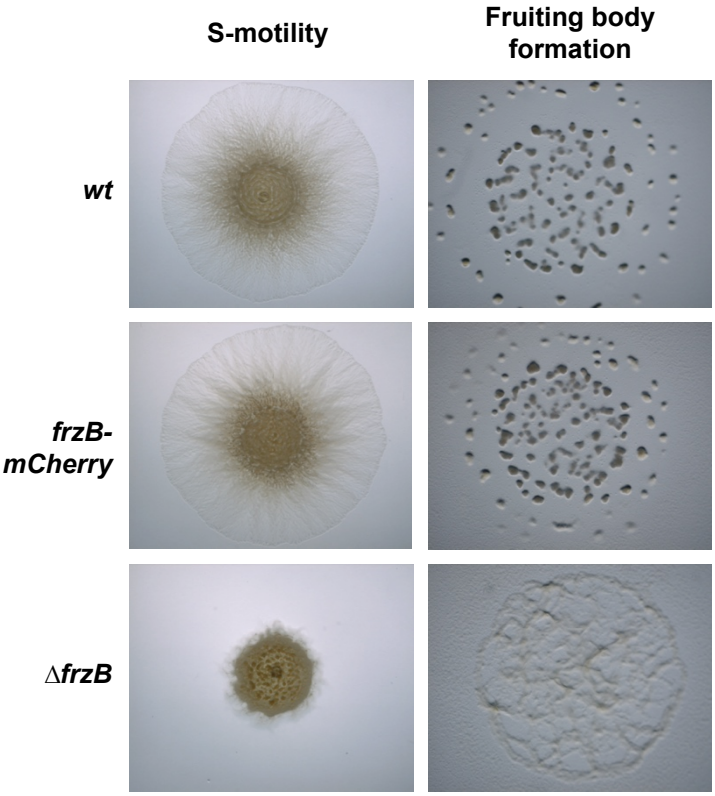
S-motility
Fruiting body formation
wt
frzB-mCherry
ΔfrzB

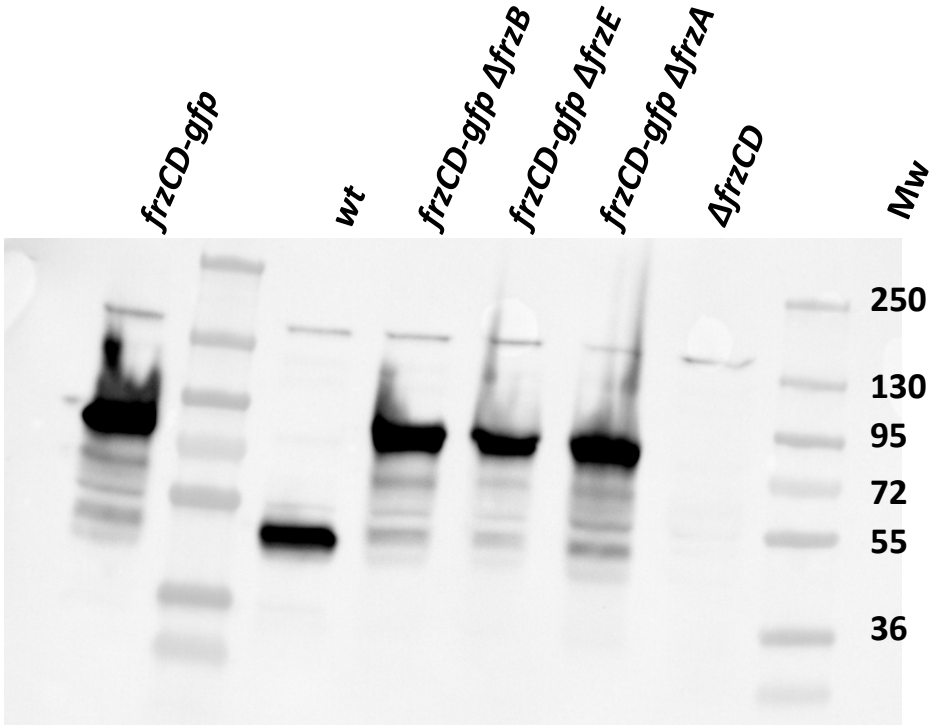
frzCD-gfp
wt
frzCD-gfp ΔfrzB
frzCD-gfp ΔfrzE
frzCD-gfp ΔfrzA
ΔfrzCD
Mw
250
130
95
72
55
36